



# Discharge/charge characteristic of Li-air cells using carbon-supported $\text{LaMn}_{0.6}\text{Fe}_{0.4}\text{O}_3$ as an electrocatalyst



Masayoshi Yuasa <sup>a,\*</sup>, Tsubasa Matsuyoshi <sup>b</sup>, Tetsuya Kida <sup>a</sup>, Kengo Shimano <sup>a</sup>

<sup>a</sup> Department of Energy and Material Sciences, Faculty of Engineering Sciences, Kyushu University, 6-1 Kasuga-koen, Kasuga-shi, Fukuoka 816-8580, Japan

<sup>b</sup> Department of Molecular and Material Sciences, Interdisciplinary Graduate School of Engineering Sciences, Kyushu University, 6-1 Kasuga-koen, Kasuga-shi, Fukuoka 816-8580, Japan

## HIGHLIGHTS

- A carbon-supported  $\text{LaMn}_{0.6}\text{Fe}_{0.4}\text{O}_3$  nanoparticle was synthesized.
- $\text{LaMn}_{0.6}\text{Fe}_{0.4}\text{O}_3$  exhibited the oxygen reduction activity for Li-air cell.
- $\text{LaMn}_{0.6}\text{Fe}_{0.4}\text{O}_3$  also exhibited the oxygen evolution activity for Li-air cell.
- Discharge capacity of Li-air cell depended on the structure of air electrode.
- Oxygen diffusion into air electrode is important for the excellent Li-air cells.

## ARTICLE INFO

### Article history:

Received 10 April 2013

Received in revised form

17 May 2013

Accepted 18 May 2013

Available online 29 May 2013

### Keywords:

Li-air cell

Oxygen reduction

Oxygen evolution

Perovskite-type oxide

Gas diffusion

## ABSTRACT

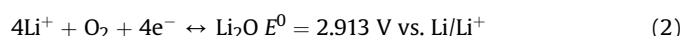
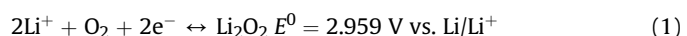
The discharge/charge performance of Li-air cell using the carbon-supported  $\text{LaMn}_{0.6}\text{Fe}_{0.4}\text{O}_3$  nanoparticle as a cathode catalyst was investigated in this study. The carbon-supported  $\text{LaMn}_{0.6}\text{Fe}_{0.4}\text{O}_3$  nanoparticle was prepared via a reverse homogeneous precipitation method, and fabricated to air electrode. Li-air cell was constructed using air electrode, Li metal foil and 1.0 M  $\text{LiPF}_6$  in propylene carbonate as a cathode, anode and electrolyte, respectively. As the result, the carbon-supported  $\text{LaMn}_{0.6}\text{Fe}_{0.4}\text{O}_3$  nanoparticle exhibited both the oxygen evolution activity and the oxygen reduction activity in the non-aqueous electrolyte. The investigation about the presence and absence of the catalytic layer and the gas diffusion layer revealed that each layer is indispensable for the excellent electrode performance, and that the catalytic layer and the gas diffusion layer has a important role to supply the electrolyte and the oxygen gas, respectively. The investigation about the amount of the catalytic layer and the effect of the oxygen concentration revealed that the oxygen diffusability into the air electrode strongly affects to the discharge capacity of Li-air cells.

© 2013 Elsevier B.V. All rights reserved.

## 1. Introduction

Metal-air batteries utilize non-noble metals (Fe [1], Zn [2], Al [3], Mg [4], Li [5]) and an atmospheric oxygen as an anode and a cathode materials, respectively. Therefore, metal-air batteries can be attractive power sources of electric vehicles and storages of renewable energies such as wind-powered electricity and photovoltaic power generation because of its high energy density. Especially, Li-air cells have largest theoretical energy density of 13,000 Wh kg<sup>-1</sup> [6] because the lithium has the lowest equilibrium electrode potential (−3.05 V vs. NHE) and the lowest density among all metals (0.534 g cm<sup>-3</sup>). A typical Li-air cell is composed of

a lithium metal, an electrolyte and a porous-structured air electrode. The electrolyte is organic solvents or ionic liquids with lithium salts such as  $\text{LiPF}_6$  and  $\text{LiOCl}_4$  [7,8]. Usually, the air electrode is composed of a catalytic layer and a gas diffusion layer. During the discharge reaction, the atmospheric oxygen diffuses into the catalytic layer through the gas diffusion layer and reduced to oxide ions ( $\text{O}_2^-$  or  $\text{O}^{2-}$ ). The oxide ions react with lithium ions in the electrolyte, and then lithium oxides ( $\text{Li}_2\text{O}$ ) or lithium peroxides ( $\text{Li}_2\text{O}_2$ ) are produced in the pores of the air electrode [9]. The electrochemical equation and equilibrium electrode potential for the formation of  $\text{Li}_2\text{O}$  and  $\text{Li}_2\text{O}_2$  during discharge reaction are the followings [10–12]:



\* Corresponding author. Tel.: +81 92 583 7539; fax: +81 92 583 7538.

E-mail address: [yuasa@mm.kyushu-u.ac.jp](mailto:yuasa@mm.kyushu-u.ac.jp) (M. Yuasa).

Recently, it has been reported that discharge reaction in Li-air cells also produces lithium carbonate ( $\text{Li}_2\text{CO}_3$ ) [13] or lithium carboxides ( $\text{HCO}_2\text{Li}$ ,  $\text{CH}_3\text{CO}_2\text{Li}$  and  $\text{C}_3\text{H}_6(\text{OCO}_2\text{Li})_2$ ) [14]. As the discharge reaction proceeds, discharge products are formed in the pores of the air electrode one after another. Finally, when discharge products fill up the all of the pores, the discharge reaction is finished because the oxygen cannot diffuse into the catalytic layer any more. During the charge reaction, lithium oxides in the pores are reversibly oxidized to  $\text{Li}^+$  and  $\text{O}_2$ , and thus the air electrode is restored for next discharge reactions.

In order to improve the discharge/charge voltage and the discharge capacity of Li-air cells, investigations about the air electrode have been numerously carried out. It has been reported that loading of an electrocatalyst is effective to improve the discharge/charge voltage and the discharge capacity. For the electrocatalyst, metals [15–17], metal oxides [18–22], composites of oxide and noble metal [23], graphene [24] and  $\text{CF}_x$  [20] have been reported. Moreover, it has been reported that a control of electrode structures is effective to improve the discharge capacity. Zheng et al. have theoretically elucidated that the discharge capacity of Li-air cell increases with an increase in a porosity of air electrodes [25].

In this work, we focused on the La-Mn-based perovskite-type oxide as an oxygen reduction catalyst for Li-air cells using the non-aqueous electrolyte. Perovskite-type oxides have widely been investigated as an oxygen reduction catalyst in the alkaline aqueous solution [26–28] since Meadowcroft first pointed out the potentiality of it [29]. In particular, we tried to disperse nanoparticles of La-Mn-based perovskite-type oxides on the carbon-support in order to increase the catalytic reaction site for oxygen reduction. This attempt achieved the highly active oxygen reduction electrode for the metal-air battery using aqueous alkaline electrolyte as compared with the electrode using a carbon-supported Pt nanoparticle [30,31]. Therefore, in this work, we attempt to apply the La-Mn-based perovskite-type oxide as an oxygen reduction catalyst of the Li-air cell using the non-aqueous electrolyte. As a La-Mn-based perovskite-type oxide,  $\text{LaMn}_{0.6}\text{Fe}_{0.4}\text{O}_3$  was chosen due to its stability against cathodic polarization as reported in our previous report [32]. In addition, we investigated a structure of air electrode in order to improve the discharge capacity of Li-air cell. The order of the catalytic layer and the gas diffusion layer, the amount of the catalytic layer per unit area, and the effect of oxygen concentration on the discharge capacity were investigated in order to elucidate the correlation between the structure of air electrode and the oxygen diffusion into air electrode.

## 2. Experimental

### 2.1. Chemicals

$\text{La}(\text{NO}_3)_3 \cdot 6\text{H}_2\text{O}$ ,  $\text{Mn}(\text{NO}_3)_2 \cdot 6\text{H}_2\text{O}$ ,  $\text{Fe}(\text{NO}_3)_3 \cdot 9\text{H}_2\text{O}$ , 10% solution of tetramethylammonium hydroxide (TMAH) and tetrapropylammonium bromide (TPAB) were purchased from Kishida chemical Co., Ltd. (Osaka, Japan) and used for the synthesis of  $\text{LaMn}_{0.6}\text{Fe}_{0.4}\text{O}_3$ . Ketjen Black (EC600JD, specific surface area:  $1280 \text{ m}^2 \text{ g}^{-1}$ ) was kindly provided by LION Co., Ltd. (Tokyo, Japan) and used as a material for the catalytic layer. Acetylene black (AB-7, specific surface area:  $47 \text{ m}^2 \text{ g}^{-1}$ ) was kindly provided by DENKI KAGAKU KOGYO KABUSHIKI KAISHA (Tokyo, Japan) and used as a material for the gas diffusion layer. Polytetrafluoroethylene (PTFE) dispersion (Polyflon TFE Series D-1) was purchased from DAIKIN INDUSTRIES, Ltd. (Osaka, Japan) and used as a binder of electrode materials. Li metal foil was purchased from Honjo Metal Co., Ltd. (Higashiosaka, Japan). 1.0 M  $\text{LiPF}_6$  in propylene carbonate was purchased from Kishida Chemical Co., Ltd. and used as an electrolyte. All chemicals were used as received without further purifications.

### 2.2. Material synthesis

The carbon-supported  $\text{LaMn}_{0.6}\text{Fe}_{0.4}\text{O}_3$  was prepared by a reverse homogeneous precipitation (RHP) method as reported in elsewhere [33,34]. At first, an aqueous solution of  $\text{La}(\text{NO}_3)_3$ ,  $\text{Mn}(\text{NO}_3)_2$  and  $\text{Fe}(\text{NO}_3)_3$  was placed in a burette and titrated against a 1% TMAH solution containing dissolved TPAB under vigorous stirring. The concentration of metal ions in the solution was fixed at 0.2 M. The amount of TBAH was equimolar to the metal ions in the solution. After mixing, a brown-colored precipitate was obtained immediately. The precipitate obtained was collected by filtration and re-dispersed into 2-propanol. Then, Ketjen Black EC600JD was added to the solution and dispersed under ultrasonic agitation (45 kHz) for 30 min. After the filtration and drying at 120 °C for more than 12 h, the powder obtained was calcined at 650 °C for 5 h in  $\text{N}_2$  flow (100 ml min<sup>-1</sup>) to produce the carbon-supported  $\text{LaMn}_{0.6}\text{Fe}_{0.4}\text{O}_3$ . The content of  $\text{LaMn}_{0.6}\text{Fe}_{0.4}\text{O}_3$  was fixed at 30 wt%. The carbon-supported  $\text{LaMn}_{0.6}\text{Fe}_{0.4}\text{O}_3$  obtained, a PTFE dispersion and 1-buthanol were added to de-ionized water and mixed for 1 h. The content of PTFE in the carbon-supported  $\text{LaMn}_{0.6}\text{Fe}_{0.4}\text{O}_3$  was fixed at 15 wt%. After the filtration and drying at 120 °C, a powder for the catalytic layer was finally obtained. The crystalline phase and the particle size of  $\text{LaMn}_{0.6}\text{Fe}_{0.4}\text{O}_3$  on the carbon-support were analyzed by means of a X-ray diffractmetry with  $\text{Cu K}\alpha$  radiation ( $\lambda = 1.54056 \text{ \AA}$ ) (XRD; RINT 2100, Rigaku, Tokyo, Japan) and a transmission electron microscopy (TEM; JEM-2000EX, JEOL, Tokyo, Japan), respectively. Separately, a powder for the gas diffusion layer was fabricated by mixing an acetylene black (AB-7) and PTFE. The content of PTFE in the powder was fixed at 30 wt%. The specific surface area of the powder for the catalytic layer and the gas diffusion layer were evaluated by means of a nitrogen adsorption/desorption apparatus (BELSORP-mini, BEL JAPAN, Inc., Osaka, Japan).

### 2.3. Electrode fabrication and cell measurements

Powders for the catalytic layer and the gas diffusion layer were stacked on the Ni mesh (100 mesh) and pressed into sheets under the pressure of 2.0 MPa. Then the stacked sheets were bound together by hot-pressing under the pressure of 5.2 MPa at 365 °C to produce air electrodes of 16 mm in diameter. The pore size distribution and pore volume of the catalytic layer and the gas diffusion layer were measured by means of a mercury porosimetry (Pore Sizer 9320, Shimadzu, Kyoto, Japan). The air electrode obtained, Li foil and electrolyte (1.0 M  $\text{LiPF}_6$  in propylene carbonate) were fabricated to Li-air cells. Fig. 1 shows the schematic cell

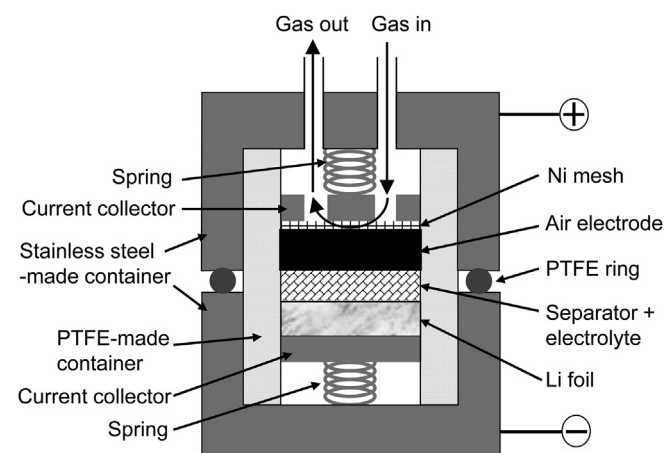


Fig. 1. Schematic cell configuration of Li-air batteries.

configuration of Li-air cells. A current collector with spring, a Li metal foil of 0.3 mm in thickness and 20 mm in diameter, and a separator (PP3501, Hohsen Co., Osaka, Japan) was stacked in the PTFE-made container. Next, 0.7 ml of an electrolyte was poured in the PTFE container. Then, the air electrode and a current collector were stacked in the PTFE-made container. The current collector on the air electrode has 4 holes in order to supply oxygen. Finally, the above assembly in the PTFE-made container was sealed up by the Stainless steel-made container with PTFE-ring, and 21% or 100% O<sub>2</sub> was supplied to the backside of the air electrode. The discharge/charge properties of the Li-air cell was measured under the galvanostatic condition using the potentio/galvano stat (HABF-5001, Hokuto Denko Co., Tokyo, Japan). The discharge capacity observed was normalized by the total weight of the catalytic layer.

### 3. Results and discussion

#### 3.1. Materials characterization

The crystalline size and the morphology of the carbon-supported LaMn<sub>0.6</sub>Fe<sub>0.4</sub>O<sub>3</sub> was evaluated by means XRD and TEM. Fig. 2 shows an XRD pattern of the carbon-supported LaMn<sub>0.6</sub>Fe<sub>0.4</sub>O<sub>3</sub> synthesized through the RHP method. The XRD pattern matches with the perovskite-phase of orthorhombic system (JCPDS 35-1353) without any other impurity phases. The crystalline size of LaMn<sub>0.6</sub>Fe<sub>0.4</sub>O<sub>3</sub> calculated by the Scherer's formula from the XRD pattern is 17.4 nm. Fig. 3 shows a TEM micrograph of the carbon-supported LaMn<sub>0.6</sub>Fe<sub>0.4</sub>O<sub>3</sub>. Since the TEM micrograph in Fig. 3 is a bright-field image, strong dark areas and weak dark areas indicate the presence of LaMn<sub>0.6</sub>Fe<sub>0.4</sub>O<sub>3</sub> and carbon-support, respectively. It was found that LaMn<sub>0.6</sub>Fe<sub>0.4</sub>O<sub>3</sub> particles of 15–20 nm in diameter are dispersed on the carbon-support. The particle size of LaMn<sub>0.6</sub>Fe<sub>0.4</sub>O<sub>3</sub> shown in the TEM image is in good agreement with the crystalline size calculated from the peak width of XRD pattern (17.4 nm). This tendency indicates that LaMn<sub>0.6</sub>Fe<sub>0.4</sub>O<sub>3</sub> particles obtained are loaded on the carbon-support as mono-crystal.

Pore structures and surface areas of the catalytic layer and the gas diffusion layer were evaluated by means of a mercury porosimetry and a nitrogen adsorption/desorption apparatus. Fig. 4 shows the pore size distribution of the gas diffusion layer and catalytic layers measured by the mercury porosimetry. Table 1 summarizes the total pore volume and the specific surface area of each layer measured by the mercury porosimetry and the nitrogen

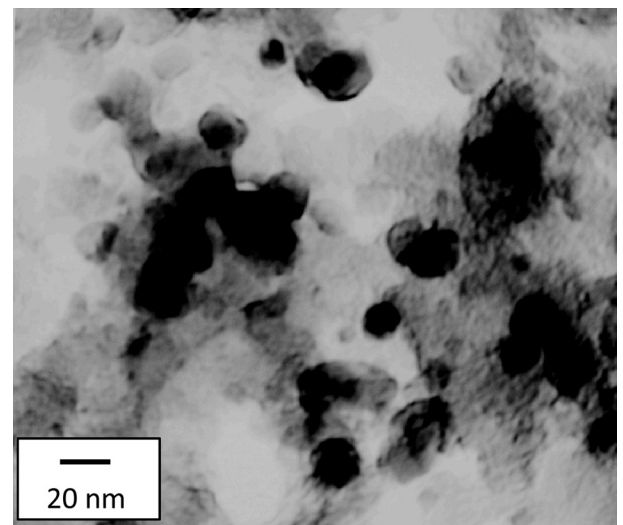


Fig. 3. TEM image of the carbon-supported LaMn<sub>0.6</sub>Fe<sub>0.4</sub>O<sub>3</sub> synthesized through the RHP method.

adsorption/desorption apparatus, respectively. As shown in Fig. 4, the gas diffusion layer has a peak of pore size distribution at 58 nm. It seems that submicron-sized and uniform pore size distribution of the gas diffusion layer serves a good oxygen pathway. On the other hand, in the case of catalytic layers, there are no typical peaks of the pore size distribution, and the pore volume increases with a decrease in the pore size. Such a tendency of catalyst layers seems to result in lower oxygen permeability as compared with the gas diffusion layer. However, as shown in Table 1, catalytic layers have larger total pore volume as compared with the gas diffusion layer. In addition, the layer with larger specific surface area tends to have larger total pore volume. Such a large pore volume can serve the storage site of discharge products in large amount.

#### 3.2. Effect of LaMn<sub>0.6</sub>Fe<sub>0.4</sub>O<sub>3</sub> loading as an electrocatalyst

Fig. 5 shows discharge curves of Li-air cells using the carbon-supported LaMn<sub>0.6</sub>Fe<sub>0.4</sub>O<sub>3</sub> and only the carbon-support as the catalytic layer. The amount of catalytic layer for each samples were

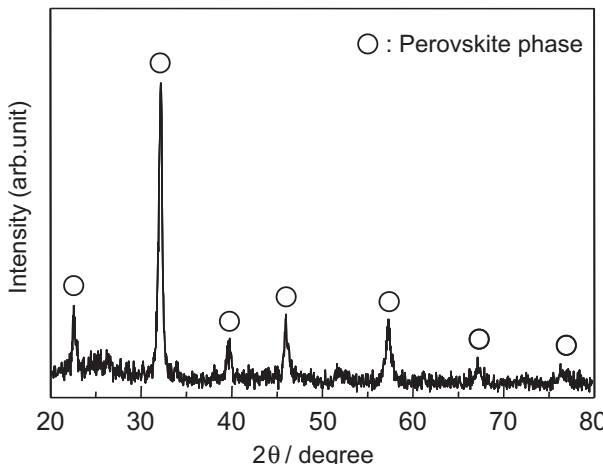


Fig. 2. XRD pattern of the carbon-supported LaMn<sub>0.6</sub>Fe<sub>0.4</sub>O<sub>3</sub> synthesized through the RHP method.

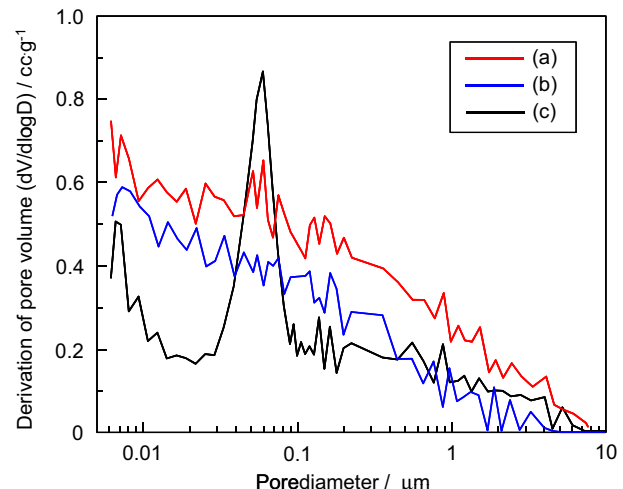


Fig. 4. Pore size distributions of (a) catalytic layer using carbon-supported LaMn<sub>0.6</sub>Fe<sub>0.4</sub>O<sub>3</sub>, (b) catalytic layer using only carbon-support and (c) gas diffusion layer.

**Table 1**

Total pore volumes and specific surface areas of electrode layers.

	Total pore volume (cc g <sup>-1</sup> )	Specific surface area (m <sup>2</sup> g <sup>-1</sup> )
Catalytic layer (carbon-supported LaMn <sub>0.6</sub> Fe <sub>0.4</sub> O <sub>3</sub> )	0.8470	566
Catalytic layer (carbon only)	1.3157	910
Gas diffusion layer	0.6694	26

fixed at 14.16 g cm<sup>-2</sup>. The discharge voltage of the air electrode using the carbon-supported LaMn<sub>0.6</sub>Fe<sub>0.4</sub>O<sub>3</sub> is higher than that of the air electrode using only the carbon-support. This result indicates that LaMn<sub>0.6</sub>Fe<sub>0.4</sub>O<sub>3</sub> can work as an oxygen reduction catalyst even in the non-aqueous electrolyte as well as in the alkaline aqueous solution. According to the reports about the oxygen reduction activity of MnO<sub>2</sub> in the non-aqueous electrolyte [18,19], it seems that Mn<sup>3+</sup> or Mn<sup>4+</sup> ions of the surface of LaMn<sub>0.6</sub>Fe<sub>0.4</sub>O<sub>3</sub> particles acted as active sites for oxygen reduction reaction. Fig. 6 shows discharge/charge cycles of Li-air cells using the carbon-supported LaMn<sub>0.6</sub>Fe<sub>0.4</sub>O<sub>3</sub> and the carbon-support only as the catalytic layer. In the case of the air electrode using the carbon-support only, the transient of charge voltage are unstable. The unstable transient of the charge voltage may correspond to the oxidation of the carbon-support by the anodic polarization [35]. The corrosion of carbon-support by the anodic polarization continuously degraded the air electrode with charge time and discharge/charge cycles, leading to a decrease in the active site for the electrochemical reaction and a large decline in the discharge voltage as seen in the 4th cycles. Contrary, in the case of the air electrode using the carbon-supported LaMn<sub>0.6</sub>Fe<sub>0.4</sub>O<sub>3</sub>, the discharge/charge voltage is quite stable during four times of discharge/charge cycles. Hayashi et al. has reported that the La-Mn-based perovskite-type oxide, La<sub>0.6</sub>Sr<sub>0.4</sub>Fe<sub>0.6</sub>Mn<sub>0.4</sub>O<sub>3</sub>, can act as an oxygen evolution catalyst [22]. Therefore, it seems that LaMn<sub>0.6</sub>Fe<sub>0.4</sub>O<sub>3</sub> also acted as an oxygen evolution catalyst, and that the oxygen evolution activity of the LaMn<sub>0.6</sub>Fe<sub>0.4</sub>O<sub>3</sub> resulted in preventing the carbon-support from anodic oxidation. Above results suggest that LaMn<sub>0.6</sub>Fe<sub>0.4</sub>O<sub>3</sub> has a role to improve both the discharge and charge properties of Li-air cell due to its oxygen reduction and oxygen evolution activity.

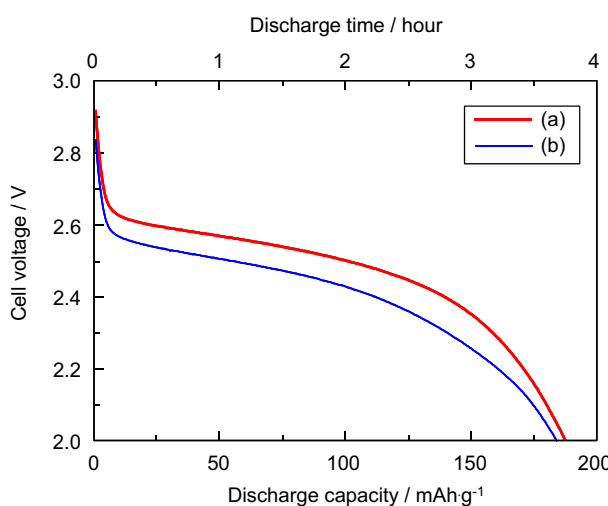


**Fig. 5.** Discharge curve of Li-air cells using (a) carbon-supported LaMn<sub>0.6</sub>Fe<sub>0.4</sub>O<sub>3</sub> and (b) the carbon-support only. All tests were carried out under the air flow at a current density of 0.5 mA cm<sup>-2</sup>.

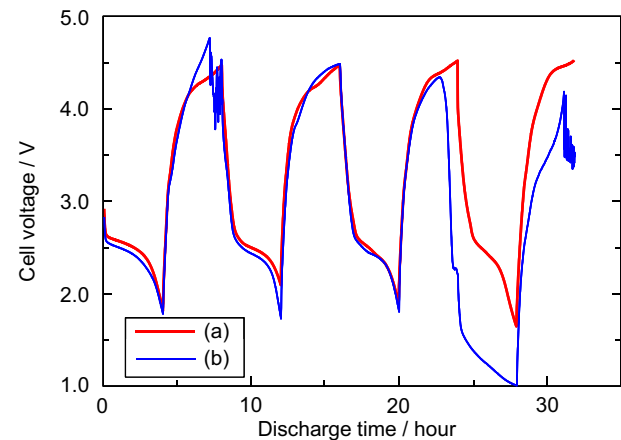


**Fig. 6.** Discharge/charge cycles of Li-air cells using (a) carbon-supported LaMn<sub>0.6</sub>Fe<sub>0.4</sub>O<sub>3</sub> and (b) carbon-support only. All tests were carried out under the air flow at a current density of 0.5 mA cm<sup>-2</sup>.

### 3.3. Effect of electrode structures on discharge performance of Li-air cells

The effect of the structure of air electrode on discharge properties of Li-air cells was investigated. At first, the meaning of the catalyst layer and the gas diffusion layer was investigated by measuring the discharge capacity of Li-air cells using various types of air electrode. Fig. 7 shows discharge curves of Li-air cells using the bi-layer of the gas diffusion layer and the catalytic layer (usual air electrode), only the gas diffusion layer and only the catalytic layer. In the Li-air cell using only the gas diffusion layer, the discharge capacity was normalized by the total weight of the gas diffusion layer. The Li-air cell using only the catalytic layer exhibited larger discharge capacity than that of only the gas diffusion layer. As shown in Fig. 4 and Table 1, the catalytic layer has larger total pore volume as compared with the gas diffusion layer. Therefore, the catalytic layers can storage the larger amount of discharge products, resulting in the larger discharge capacity. Moreover, it seems that the difference in the wettability for electrolytes affected to the difference in the discharge capacity, because wettability for the electrolyte of electrode materials affects to the mixing state of

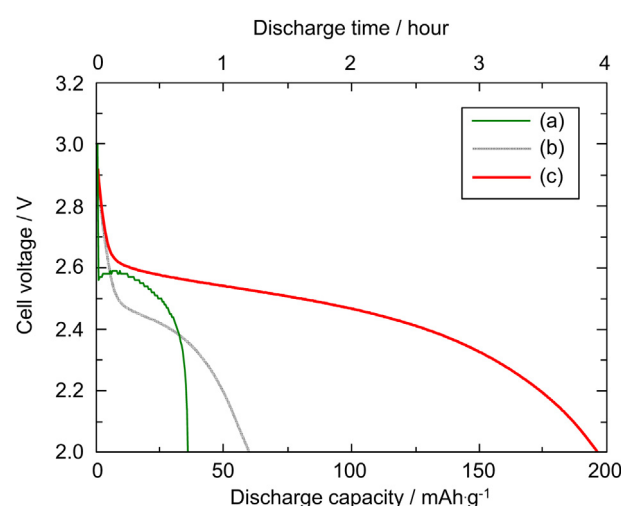


**Fig. 7.** Discharge curves of Li-air cells using (a) gas diffusion layer only, (b) catalytic layer only and (c) bi-layer of catalytic layer and gas diffusion layer (usual air electrode). All tests were carried out under the air flow at a current density of 0.5 mA cm<sup>-2</sup>.

electrolyte and oxygen in air electrodes. The mixing state of oxygen and electrolyte is very important factor because the oxygen reduction reaction proceeds at three-phase boundary which involves the oxygen, the electrolyte and the electrode material. Therefore, the wettability of each layer was evaluated by measuring the contact angle of the electrolyte on the electrode layers. At first, an electrolyte droplet of 1.5 mm in diameter was placed on electrode layers using a micromanipulator (PatchMan NP2, Eppendorf Co., Ltd., Hamburg, Germany). Then the contact angle of the electrolyte on electrode layers was measured at room temperature. As the result, the contact angle of the electrolyte on the gas diffusion layer and the catalyst layer was  $110.5^\circ$  and  $56.0^\circ$ , respectively. This result indicates that the catalytic layer has larger wettability as compared with the gas diffusion layer. Therefore, the electrolyte is easy to penetrate the catalytic layer, and difficult to penetrate the gas diffusion layer. Thus, the gas diffusion layer has smaller amount of the reaction site for discharge reaction as compared with the catalytic layer, leading to the low charge capacity of the air electrode using only the gas diffusion layer. The discharge capacity of the Li-air cell using bi-layer electrode was much larger than that of only the catalytic layer only. In the case of the air electrode using only the catalyst layer, the electrolyte occupies the large portion of the air electrode because wettability of the catalytic layer is higher than that of the gas diffusion layer, thereby resulted in the low discharge capacity of the air electrode using only the catalytic layer as compared with bi-layer electrode. Contrary, in the case of bi-layer electrode, the ratio of oxygen to electrolyte may be well balanced by combining the oxygen-rich gas diffusion layer and the electrolyte-rich catalyst layer, resulting in high discharge capacity. The above results indicate that both the catalytic layer and the gas diffusion layer are indispensable for the excellent electrode performance.

The effect of the amount of catalytic layer on the discharge capacity of Li-air cells was then investigated. Fig. 8 shows discharge curves of Li-air cells using various amount of carbon-supported  $\text{LaMn}_{0.6}\text{Fe}_{0.4}\text{O}_3$  as the catalytic layer. The discharge duration of Li-air cells is increased with an increase in the content of catalytic layer, because the amount of storage space of discharge product increase with an increase in the total pore volume in the catalytic layer. However, when the discharge curves of Fig. 8 is re-plotted as a function of the charge capacity, the discharge capacity of Li-air cells decreases with an increase in the content of catalyst layer as shown in Fig. 9. The increase in the amount of catalyst layer will increase

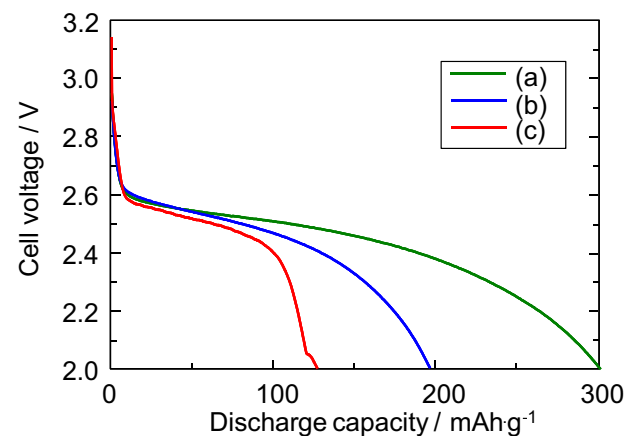


Fig. 9. Re-plotting of discharge curves in Fig. 8 as a function of the discharge capacity.

the total pore volume. Therefore, it is generally expected that the discharge capacity increases with the increase in the amount of catalyst layer. However, the result obtained was opposite to the expected tendency. When the catalyst layer is too thick, oxygen may be difficult to diffuse into deep part of the catalyst layer. In this case, most of oxygen is consumed at the region near the gas diffusion layer before the oxygen diffuses into the deep part of the catalyst layer. Therefore, discharge products were maldistributed at the region near the gas diffusion layer, and thus the discharge products obstructed the oxygen diffusion into deep part of catalyst layer. Consequently, the discharge reaction of Li-air cell was finished without forming discharge products at the deep part of catalyst layer. Fig. 10 shows the effect of the oxygen concentration on discharge curves of Li-air cells. The catalyst layer was the carbon-supported  $\text{LaMn}_{0.6}\text{Fe}_{0.4}\text{O}_3$  of  $14.16 \text{ g cm}^{-2}$ . As shown in Fig. 10, the Li-air cell under  $100\%$   $\text{O}_2$  flow exhibited larger discharge capacity as compared with the air flow. In general, it seems that the discharge capacity is independent on the oxygen concentration, because air batteries can discharge as long as the oxygen diffuses into the air electrode. However, in the case of our measurement under air flow, most of oxygen may be consumed at the region near the gas diffusion layer. Such a lack of oxygen in the deep part of catalyst layer caused the maldistribution of discharge products at

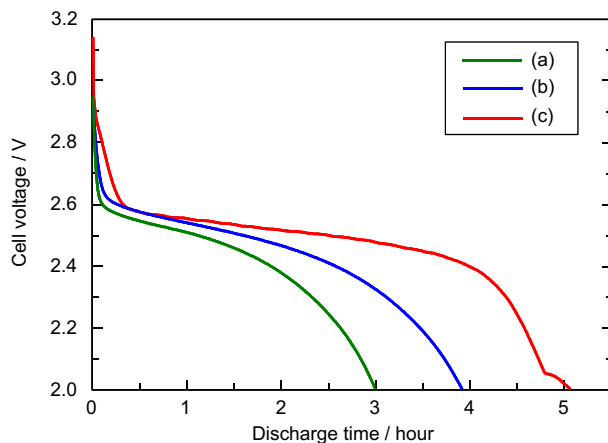


Fig. 8. Discharge curves of Li-air cells using various amount of carbon-supported  $\text{LaMn}_{0.6}\text{Fe}_{0.4}\text{O}_3$ . The content of the catalytic layer is (a)  $7.08 \text{ g cm}^{-2}$ , (b)  $14.16 \text{ g cm}^{-2}$  and (c)  $28.31 \text{ g cm}^{-2}$ . All tests were carried out under the air flow at a current density of  $0.5 \text{ mA cm}^{-2}$ .

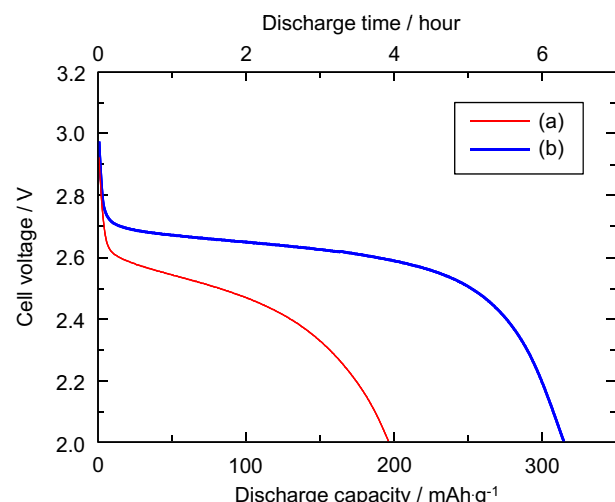


Fig. 10. Discharge curves of Li-air cells using carbon-supported  $\text{LaMn}_{0.6}\text{Fe}_{0.4}\text{O}_3$  as a catalytic layer under (a)  $21\%$   $\text{O}_2$  flow and (b)  $100\%$   $\text{O}_2$  flow at a current density of  $0.5 \text{ mA cm}^{-2}$ .

the region near the gas diffusion layer, and then the discharge reaction was finished without forming the discharge products at the deep part of the catalyst layer. Contrary, in the case of 100% O<sub>2</sub> flow, adequate amount of oxygen was supplied in the whole region of the catalyst layer, and thus the whole region of the catalyst layer could storage discharge products. According to above results, the catalyst layer which has large thickness and good oxygen pathway is required for the Li-air cell with large discharge capacity.

#### 4. Conclusion

In order to improve the discharge/charge voltage and discharge capacity of Li-air cells, an effect of LaMn<sub>0.6</sub>Fe<sub>0.4</sub>O<sub>3</sub> addition on the catalytic layer of the air electrode and a structure of air electrode was investigated. It was found that the LaMn<sub>0.6</sub>Fe<sub>0.4</sub>O<sub>3</sub> nanoparticle can increase the discharge voltage of Li-air cell. Moreover, the LaMn<sub>0.6</sub>Fe<sub>0.4</sub>O<sub>3</sub> had an effect to stabilize the charge reaction of Li-air cell due to its oxygen evolution activity. The investigation about the meaning of the catalytic layer and the gas diffusion layer revealed that the catalytic layer and the gas diffusion layer have a important role to feed the electrolyte and the oxygen, respectively. Consequently, the mixing state of electrolyte and oxygen in the air electrode was well optimized, resulting in an excellent discharge capacity. As the result of investigations about the content of catalytic layer and the oxygen concentration, it was found that oxygen consumed at the outside of catalytic layer when the catalytic layer is too thick or the oxygen concentration is low. Such an insufficient supply of oxygen into the deep part of the catalytic layer air caused the maldistributin of the discharge products. In order to increase the discharge capacity of the Li-air cell, structural optimizations of air electrode for the adequate oxygen diffusion are required.

#### References

- [1] B.T. Hang, M. Egashira, I. Watanabe, S. Okada, J.-I. Yamaki, S.-H. Yoon, I. Mochida, *J. Power Sources* 143 (2005) 256–264.
- [2] A.J. Appleby, M. Jacquier, *J. Power Sources* 1 (1976) 17–34.
- [3] S. Yang, H. Knickle, *J. Power Sources* 112 (2002) 162–173.
- [4] S. Sathanarayana, N. Munichandraiah, *J. Appl. Electrochem.* 11 (1981) 33–39.
- [5] K.M. Abraham, Z. Jiang, *J. Electrochem. Soc.* 143 (1996) 1–5.
- [6] D. Linden, T. Reddy, *Handbook of Batteries*, third ed., McGraw Hill, New York, 2001.
- [7] W. Xu, J. Xiao, J. Zhang, D. Wang, J.-G. Zhang, *J. Electrochem. Soc.* 156 (2009) A773–A779.
- [8] H. Ye, J. Huang, J.-J. Xu, A. Khalfan, S.G. Greenbaum, *J. Electrochem. Soc.* 154 (2007) A1048–A1057.
- [9] M. Eswaran, N. Munichandraiah, L.G. Scanlon, *Electrochem. Solid-State Lett.* 13 (2010) A121–A124.
- [10] A. Kraytsberg, Y. Ein-Eli, *J. Power Sources* 196 (2011) 886–893.
- [11] Y. Yang, Q. Sun, Y.-S. Li, H. Li, Z.-W. Fu, *J. Electrochem. Soc.* 158 (2011) B1211–B1216.
- [12] J.-S. Lee, S.T. Kim, R. Cao, N.-S. Choi, M. Liu, K.T. Lee, J. Cho, *Adv. Energy Mater.* 1 (2011) 34–50.
- [13] J. Xiao, J. Hu, D. Wang, D. Hu, W. Xu, G.L. Graff, Z. Nie, J. Liu, J.-G. Zhang, *J. Power Sources* 196 (2011) 5674–5678.
- [14] S.H. Freunberger, Y. Chen, Z. Peng, J.M. Griffin, L.J. Hardwick, F. Bardé, P. Novák, P.G. Bruce, *J. Am. Chem. Soc.* 133 (2011) 8040–8047.
- [15] Y.-C. Lu, Z. Xu, H.A. Gasteiger, S. Chen, K. Hamad-Schifferli, Y. Shao-Horn, *J. Am. Chem. Soc.* 132 (2010) 12170–12171.
- [16] Y.-C. Lu, H.A. Gasteiger, E. Crumlin, R. McGuire Jr., Y. Shao-Horn, *J. Electrochem. Soc.* 157 (2010) A1016–A1025.
- [17] S.S. Zhang, X. Ren, J. Read, *Electrochim. Acta* 56 (2011) 4544–4548.
- [18] A. Débart, A.J. Paterson, J. Bao, P.G. Bruce, *Angew. Chem., Int. Ed.* 47 (2008) 4521–4524.
- [19] K.B. Chung, J.K. Shin, T.Y. Jang, D.K. Noh, Y. Tak, S.-H. Baeck, *Rev. Adv. Mater. Sci.* 28 (2011) 54–58.
- [20] J. Xiao, W. Xu, D. Wang, J.-G. Zhang, *J. Electrochem. Soc.* 157 (2010) A294–A297.
- [21] T.H. Yoon, Y.J. Park, *Nanoscale Res. Lett.* 7 (2012) 1–11.
- [22] H. Minowa, M. Hayashi, M. Takahashi, T. Shodai, *Electrochemistry* 78 (2010) 353–356.
- [23] A.K. Thapa, K. Saimen, T. Ishihara, *Electrochem. Solid-State Lett.* 13 (2010) A165–A167.
- [24] E. Yoo, H. Zhou, *ACS Nano* 5 (2011) 3020–3026.
- [25] J.P. Zheng, R.Y. Liang, M. Hendrickson, E.J. Plichta, *J. Electrochem. Soc.* 155 (2008) A432–A437.
- [26] Y. Shimizu, K. Uemura, H. Matsuda, N. Miura, N. Yamazoe, *J. Electrochem. Soc.* 137 (1990) 3430–3433.
- [27] S. Müller, K. Striebel, O. Haas, *Electrochim. Acta* 39 (1994) 1661–1668.
- [28] T. Hyodo, M. Hayashi, N. Miura, N. Yamazoe, *J. Electrochem. Soc.* 143 (1996) L266–L267.
- [29] D.B. Meadowcroft, *Nature* 226 (1970) 847–848.
- [30] M. Yuasa, G. Sakai, K. Shimano, Y. Teraoka, N. Yamazoe, *J. Electrochem. Soc.* 151 (2004) A1690–A1695.
- [31] M. Yuasa, K. Shimano, Y. Teraoka, N. Yamazoe, *Electrochem. Solid-State Lett.* 14 (2011) A67–A69.
- [32] M. Yuasa, N. Yamazoe, K. Shimano, *J. Electrochem. Soc.* 158 (2011) A411–A416.
- [33] Y. Teraoka, S. Nanri, I. Moriguchi, S. Kagawa, K. Shimano, N. Yamazoe, *Chem. Lett.* 29 (2000) 1202–1203.
- [34] S. Imaizumi, K. Shimano, Y. Teraoka, N. Miura, N. Yamazoe, *J. Electrochem. Soc.* 51 (2004) A1559–A1564.
- [35] P.N. Ross, H. Sokol, *J. Electrochem. Soc.* 131 (1984) 1742–1750.